

Design of sextuple-mode triple-ring HTS UWB filter using two-round interpolation

Ming-En Tian(田明恩), Zhi-He Long(龙之河), You Lan(蓝友), Lei-Lei He(贺磊磊), Tian-Liang Zhang(张天良)

Citation: Chin. Phys. B, 2021, 30 (**5**): 058503. DOI: 10.1088/1674-1056/abd7e1
Journal homepage: http://cpb.iphy.ac.cn; http://iopscience.iop.org/cpb

What follows is a list of articles you may be interested in

Compact ultra-narrowband superconducting filter using N-spiral resonator with open-loop secondary coupling structure

Lin Tao(陶琳), Bin Wei(魏斌), Xubo Guo(郭旭波), Hongcheng Li(李宏成), Chenjie Luo(骆晨杰), Bisong Cao(曹必松), Linan Jiang(姜立楠)
Chin. Phys. B, 2020, 29 (**6**): 068502. DOI: 10.1088/1674-1056/ab888d

Compact high-order quint-band superconducting band-pass filter

Di Wu(吴荻), Bin Wei(魏斌), Xi-Long Lu(陆喜龙), Xin-Xiang Lu(卢新祥), Xu-Bo Guo(郭旭波), Bi-Song Cao(曹必松)
Chin. Phys. B, 2018, 27 (**6**): 068503. DOI: 10.1088/1674-1056/27/6/068503

Compact wide stopband superconducting bandpass filter using modified spiral resonators with interdigital structure

Di Wu(吴荻), Bin Wei(魏斌), Bo Li(李博), Xu-Bo Guo(郭旭波), Xin-Xiang Lu(卢新祥), Bi-Song Cao(曹必松)
Chin. Phys. B, 2018, 27 (**6**): 068502. DOI: 10.1088/1674-1056/27/6/068502

Compact superconducting single-and dual-band filter design using multimode stepped-impedance resonator

Xiang Wang(王翔), Bin Wei(魏斌), Xi-Long Lu(陆喜龙), Xu-Bo Guo(郭旭波), Bi-Song Cao(曹必松)
Chin. Phys. B, 2017, 26 (**12**): 128501. DOI: 10.1088/1674-1056/26/12/128501

A high-temperature superconducting filter withcontrollable transmission zero

Tianqi Gao(高天琪), Bin Wei(魏斌), Yong Heng(衡勇)
Chin. Phys. B, 2017, 26 (**5**): 058503. DOI: 10.1088/1674-1056/26/5/058503

Design of sextuple-mode triple-ring HTS UWB filter using two-round interpolation*

Ming-En Tian(田明恩)[1], Zhi-He Long(龙之河)[2], You Lan(蓝友)[1], Lei-Lei He(贺磊磊)[1], and Tian-Liang Zhang(张天良)[1,†]

[1] School of Aeronautics and Astronautics, University of Electronic Science and Technology of China, Chengdu 611731, China
[2] Department of Mechanical Engineering, City University of Hong Kong, Kowloon, Hong Kong SAR, China

(Received 24 August 2020; revised manuscript received 30 November 2020; accepted manuscript online 4 January 2021)

A single-stage ring resonator capable of introducing six modes within the ultra-wideband (UWB) passband is presented. The sextuple-mode resonator consists of three rings and three sets of stepped-impedance open stubs. Based on this sextuple-mode resonator, a UWB filter fed by the interdigital-coupling line (ICL) is designed. And we propose a two-round interpolation method to obtain the filter's initial dimensions. The designed filter is fabricated on a double-sided YBCO/MgO/YBCO high-temperature superconducting (HTS) thin film for demonstration. The experimental results show that this UWB filter produces eight resonances in the passband eventually, which effectively improves the in-band reflection and the band-edge steepness. Moreover, the upper stopband performance is enhanced due to the transmission zeros (TZs) generated by the stepped-impedance open stubs and the ICL structure. The measured good performance verifies the practicability of the two-round interpolation approach, which can also be extended to other odd–even-mode filter designs.

Keywords: HTS filter, ring resonator, sextuple-mode, two-round interpolation, ultra-wideband (UWB)

PACS: 85.25.–j **DOI:** 10.1088/1674-1056/abd7e1

1. Introduction

The ultra-wideband (UWB) wireless communication system is promising because it can provide fast response speed and high positioning accuracy required by many military and civilian applications. And the UWB bandpass filter, the key building block, in the UWB system has aroused the great interest of researchers. The microstrip ring resonator with many attractive merits, including the low radiation loss, high-Q factor, compact size, split modes, and sharp rejection skirts, is widely employed in the development of the UWB bandpass filters. Ring resonators possess a variety of shapes, such as circles,[1–5] rectangles,[6–9] and triangles,[10] among which the rectangular ones have greater research value due to the easiness of design and processing. The UWB filters based on rectangular single-ring resonators have been extensively studied. However, the in-band return loss or the selectivity of the passband is not better than the counterpart of the high-order UWB filters with a larger size, due to the number of resonant modes excited by these single-stage ring resonators usually being less than six. Furthermore, the upper stopband suppression performance of the ring resonator UWB filters is still worth investigating.

In this paper, we design a compact triple-ring resonator loaded with three sets of stepped-impedance open stubs to realize a UWB filter with better return loss and upper stopband. This multi-mode resonator can give rise to six modes, and two more resonances can be generated by the interdigital-coupling line (ICL) structure.[11] The initial dimensions of the designed UWB filter are determined by the proposed practical two-round interpolation method.

2. Design of UWB filter

Figure 1 shows the proposed triple-ring sextuple-mode UWB filter working in a range of 3.1 GHz–10.6 GHz, the commercial UWB communication frequency band which is assigned by the Federal Communications Commission (FCC). The three groups of stepped-impedance open stubs are specially designed for miniaturization. Typically, the resonant modes are evenly distributed within the passband, and taking into account the effect of the transition sidebands, we allocate the six resonant modes at 3.4 GHz, 5 GHz, 6.5 GHz, 8 GHz, 9.2 GHz, and 10.4 GHz, among which the fundamental odd and even modes f_{o1} (3.4 GHz) and f_{e1} (5 GHz) are particularly important and will be used to determine the filter initial dimensions.

Since the proposed UWB filter is symmetrical in the vertical and horizontal directions, we apply the even–odd-mode method to simplifying the analysis. When considering the resonant frequencies of odd modes, the perfect electric wall can be introduced into the symmetric plane. Figure 2(a) shows an odd-mode equivalent circuit. For the calculation of even-mode resonances, the plane of symmetry can be regarded as

*Project supported by the National Natural Science Foundation of China (Grant No. 61471094).
†Corresponding author. E-mail: ztl@uestc.edu.cn
© 2021 Chinese Physical Society and IOP Publishing Ltd

the perfect magnetic wall, and the corresponding even-mode equivalent circuit is depicted in Fig. 2(b). Also, the potential of the upper and lower symmetric nodes are equal, *i.e.*, the plane of stubs loaded in the central ring can be considered as an open-circuit, and therefore the improved odd- and even-mode equivalent circuits can be obtained as shown in Figs. 2(c) and 2(d). And for the convenience of analysis, the three pairs of stepped-impedance stubs are simplified into the uniform-impedance stubs, which finally will be converted into the stepped-impedance ones again. However, these two circuits in Figs. 2(c) and 2(d) are still rather complex and difficult to analyze. They can be further simplified as shown in Figs. 2(e) and 2(f) based on the theoretical analysis of the input voltage and input current as well as the potentials.

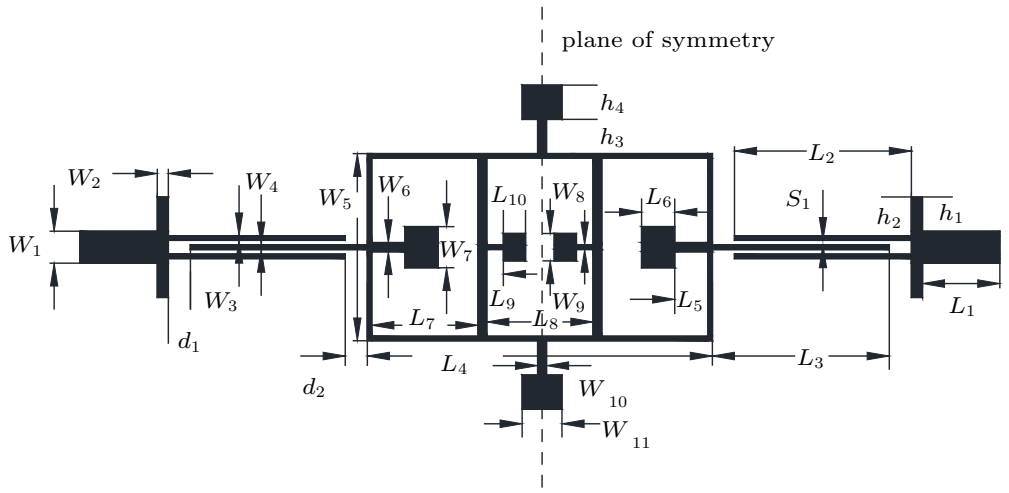


Fig. 1. Proposed sextuple-mode UWB filter layout.

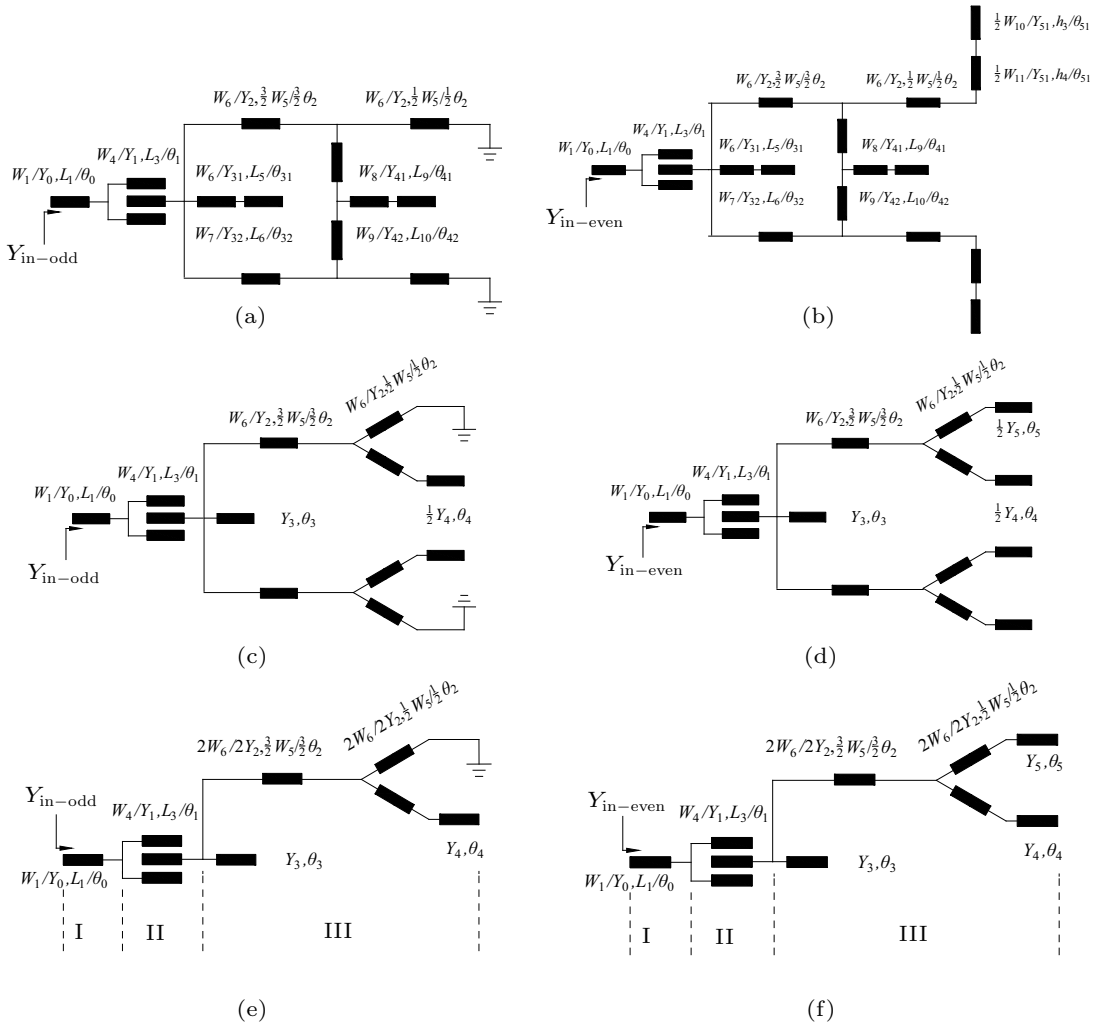


Fig. 2. Odd–even-mode analyses of [(a), (c), and (e)] odd-mode equivalent circuits and [(b), (d), and (f)] even-mode equivalent circuits.

Table 1. *ABCD* matrices for basic transmission line models.

Models	Series transmission line	Series open-circuit transmission line	Series short-circuit transmission line
ABCD matrix	$\begin{bmatrix} \cos\theta & \mathrm{j}\sin\theta/Y \\ \mathrm{j}Y\sin\theta & \cos\theta \end{bmatrix}$	$\begin{bmatrix} 1 & -\mathrm{j}\cot\theta/Y \\ 0 & 1 \end{bmatrix}$	$\begin{bmatrix} 1 & \mathrm{j}\tan\theta/Y \\ 0 & 1 \end{bmatrix}$

We utilize the *ABCD* matrices and the proposed two-round interpolation method to obtain the initial values of the filter. The *ABCD* matrices for the basic transmission line models used in this paper are listed in Table 1. According to the series transmission line models, we can calculate the transmission matrix M_{I} for the part I in Fig. 2, and the *ABCD* transmission matrix M_{II} for the ICL structure can be acquired from Ref. [12].

The core of the design method is the two-round interpolation. The first round is to determine the value for the most critical parameter by setting special values for trivial parameters to simplify the calculation and then by applying the interpolation approach under the odd- and even-mode resonance conditions. In this design, θ_2 is a key parameter. To explain why θ_2 has a greater influence on all modes than other parameters, the mathematical derivations of all modes are given in Table 2. According to the odd–even-mode analysis, the two equivalent circuits of Figs. 2(c) and 2(d) can be further simplified into those in Figs. 3(a)–3(d), respectively, because the two circuit diagrams of Figs. 2(c) and 2(d) are still symmetrical about the horizontal axis. The four resonators in Figs. 3(a)–3(d) can generate multiple resonant modes. Here, only the seven modes used in this paper are derived. None of those modes that have frequencies higher than 20 GHz but no effect on the filter is considered. It can be seen from Table 2 that only θ_2 exists in all the equations under the seven resonance conditions, which indicates that θ_2 is the most important parameter. The second round is to determine the values for some secondary parameters (θ_3, θ_4, and θ_5 here) by adjusting some preset values for trivial parameters in the first round and solving the generation conditions of transmission zeros (TZs).

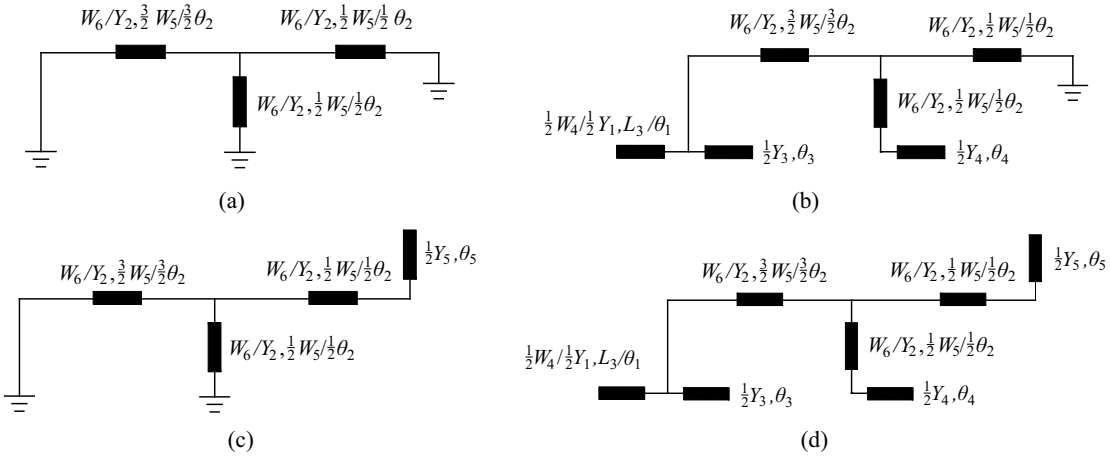
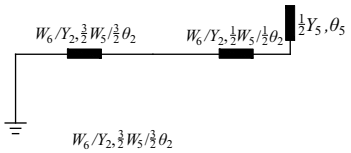
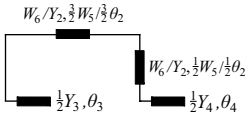
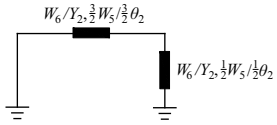
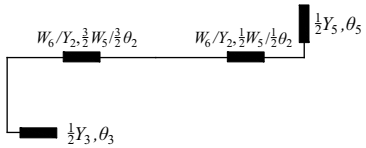
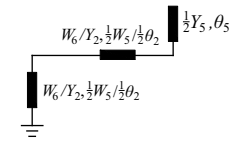
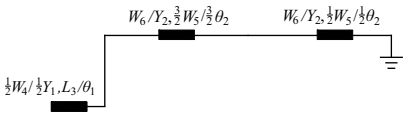
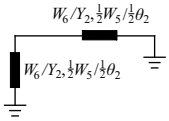


Fig. 3. Further simplified equivalent circuits based on Figs. 2(c) and 2(d).

The specific initial value acquisition process of the first-round interpolation is given below. The ring resonator is a full-wavelength resonator, so θ_2 is equal to a quarter of the wavelength corresponding to the center frequency, which is 1.59. And Y_2 is the characteristic admittance corresponding to 0.2 mm, the frequently-used microstrip line width. $Y_2 = 0.014$ S. For the convenience of description, we suppose $Y_2 = K_1Y_3 = K_2Y_4 = K_3Y_5$, $\theta_2 = B_1\theta_3 = B_2\theta_4 = B_3\theta_5 = B_4\theta_1$. To facilitate the odd–even-mode analysis, we here in this work let $K_1 = K_2 = K_3 = 2$. Then, according to the preset resonance frequencies, the odd-mode equivalent circuits in Table 2 and their resonance condition equations, B_3 can be calculated and equal to 1. Similarly, based on the preset resonance frequencies, even-mode equivalent circuits in Table 2, their resonance condition equations, and $B_3 = 1$, the remaining B_i values can be computed, namely $B_1 = 0.4$, $B_2 = 0.3$, and $B_4 = 1$. To reduce the deviation, the value of K_i and B_i are substituted into the original formulas again, and the resonance frequencies obtained are listed in Table 2. These frequency values obtained by the backward derivation are consistent with the preset frequencies. Therefore, the accuracy of K_i and B_i are guaranteed. The length of the filter ports is taken as a constant value of 3 mm for connecting ports to connecters by using the golden wire, and the width of ports is 0.48 mm corresponding to 50 Ω. For a strong coupling, the line and slot width of ICL are chosen to be 0.1 mm and 0.03 mm under the limited processing accuracy.

Table 2. Derivation of used seven resonant modes.

Finally-simplified equivalent circuit	Based on Fig. 3	Obtained mode	Corresponding resonance condition	Calculated frequency (GHz)
	(c)	f_{o1}	$Y_a = -jY_2\cot 2\theta_2$ $Y_b = Y_2\frac{-jY_2\cot 2\theta_2 + jY_2\tan B_3\theta_2}{Y_2+Y_2\cot 2\theta_2\tan B_3\theta_2} = 0$	3.40
	(b)	f_{e1}	$Y_a = jY_2\tan B_2\theta_2$ $Y_b = Y_2\frac{jY_2\tan B_2\theta_2 + jY_2\tan 2\theta_2}{Y_2-Y_2\tan B_2\theta_2\tan 2\theta_2}$ $Y_c = Y_2\frac{Y_b+jY_2\tan B_1\theta_2}{Y_2+jY_b\tan B_1\theta_2} = 0$	5.07
	(c)	f_{o2}	$\frac{1}{2}Y_2\frac{1}{j\tan(3/2)\theta_2} + Y_2\frac{1}{j\tan(1/2)\theta_2} = 0$	6.50
	(d)	f_{e2}	$Y_a = jY_2\tan B_3\theta_2$ $Y_b = Y_2\frac{jY_2\tan B_3\theta_2 + jY_2\tan 2\theta_2}{Y_2-Y_2\tan B_3\theta_2\tan 2\theta_2}$ $Y_c = Y_2\frac{Y_b+jY_2\tan B_1\theta_2}{Y_2+jY_b\tan B_1\theta_2} = 0$	8.05
	(c)	f_{o3}	$Y_a = -jY_2\cot\theta_2$ $Y_b = Y_2\frac{-jY_2\cot\theta_2 + jY_2\tan B_3\theta_2}{Y_2+Y_2\cot\theta_2\tan B_3\theta_2} = 0$	9.20
	(b)	f_{e3}	$Y_a = -jY_2\cot 2\theta_2$ $Y_b = \frac{1}{4}Y_2\frac{-jY_2\cot 2\theta_2 + j(1/4)Y_2\tan B_4\theta_2}{(1/4)Y_2+Y_2\cot 2\theta_2\tan B_4\theta_2} = 0$	10.71
	(a)	f_{o4}	$Y = 2Y_2\frac{\infty+jY_2\tan(1/2)\theta_2}{Y_2+j\infty\tan(1/2)\theta_2} = 0$	13.70

$$M_{\rm I} = \begin{bmatrix} \cos\theta_0 & \dfrac{j\sin\theta_0}{Y_0} \\ jY_0\sin\theta_0 & \cos\theta_0 \end{bmatrix}, \tag{1}$$

$$M_{\rm II} = \begin{bmatrix} \dfrac{Z_{0e}+Z_{0o}}{Z_{0e}-Z_{0o}}\cos\theta_1 & j\dfrac{(Z_{0e}+Z_{0o})^2\cos^2\theta_1 - 2(Z_{0e}-Z_{0o})^2}{4(Z_{0e}-Z_{0o})\sin\theta_1} \\ j\dfrac{2\sin\theta_1}{Z_{0e}-Z_{0o}} & (1/2)\dfrac{Z_{0e}+Z_{0o}}{Z_{0e}-Z_{0o}}\cos\theta_1 \end{bmatrix}, \tag{2}$$

$${}^{\rm III}Y^{\rm o}_{11} = j2Y_2\frac{\tan(3/2)\theta_2(1-\tan(1/2)\theta_2\tan\theta_4)+\tan(1/2)\theta_2+2\tan\theta_4-\cot(1/2)\theta_2}{(1-\tan(1/2)\theta_2\tan\theta_4)-\tan(3/2)\theta_2(\tan(1/2)\theta_2+2\tan\theta_4-\cot(1/2)\theta_2)} + j2Y_2\tan\theta_3, \tag{3}$$

$${}^{\rm III}Y^{\rm o}_{12} = {}^{\rm III}Y^{\rm o}_{21} = \frac{-j2Y_2(\tan\theta_4/\cos(1/2)\theta_2+\tan\theta_4-\cot(1/2)\theta_2)}{\cos(3/2)\theta_2(1-\tan(1/2)\theta_2\tan\theta_4)-\sin(3/2)\theta_2(\tan(1/2)\theta_2+2\tan\theta_4-\cot(1/2)\theta_2)} - j2Y_2\tan\theta_3, \tag{4}$$

$$\begin{aligned} {}^{\rm III}Y^{\rm o}_{22} = {} & -j2Y_2\{[(2\tan\theta_4-\cot(1/2)\theta_2)(\tan(1/2)\theta_2\tan\theta_4-1)-\tan(3/2)\theta_2(\tan\theta_4/\cos(1/2)\theta_2+\tan\theta_4-\cot(1/2)\theta_2)^2 \\ & +\tan(3/2)\theta_2(2\tan\theta_4-\cot(1/2)\theta_2)(\tan(1/2)\theta_2+2\tan\theta_4-\cot(1/2)\theta_2)]/[(1-\tan(1/2)\theta_2\tan\theta_4)^2-\tan(3/2)\theta_2 \\ & \times(1-\tan(1/2)\theta_2\tan\theta_4)(\tan(1/2)\theta_2+2\tan\theta_4-\cot(1/2)\theta_2)]\} + j2Y_2\tan\theta_3, \end{aligned} \tag{5}$$

$$M^{\rm o}_{\rm III} = \frac{1}{{}^{\rm III}Y^{\rm o}_{21}}\begin{bmatrix} -{}^{\rm III}Y^{\rm o}_{22} & -1 \\ {}^{\rm III}Y^{\rm o}_{12}\,{}^{\rm III}Y^{\rm o}_{21} - {}^{\rm III}Y^{\rm o}_{11}\,{}^{\rm III}Y^{\rm o}_{22} & -{}^{\rm III}Y^{\rm o}_{11} \end{bmatrix}, \tag{6}$$

$$M^{\rm o}_{[ABCD]} = M_{\rm I}\cdot M_{\rm II}\cdot M^{\rm o}_{\rm III}, \tag{7}$$

$$Y^{\rm o}_{\rm in} = \frac{M^{\rm o}_{[D]}}{M^{\rm o}_{[B]}}, \tag{8}$$

$$\theta_2 = \frac{2\pi f W_5\sqrt{\varepsilon_{\rm r}}}{c}. \tag{9}$$

The admittance matrix elements of the odd-mode circuit in Fig. 2(e) are derived from Eqs. (3)–(5) through the complex computation based on the transmission line theory and the basic model *ABCD* matrices in Table 1, and then Eqs. (6)–(8) yield the odd-mode input admittance $Y_{\rm in}^{\rm o}$ of the filter, which should satisfy $Y_{\rm in}^{\rm o}=0$ when the odd-mode resonance happens. Again, the ring resonator is a full-wavelength resonator, so according to Eq. (9), the square ring's width W_5 is calculated and equal to 3.5 mm. Subsequently, let W_5 take the value in a range from 3.0 mm to 4.0 mm in sequence in steps of 0.1 mm. It can be observed that when W_5 changes from 3.1 mm to 3.3 mm, $Y_{\rm in}^{\rm o}$ varies from -1.72j to 0.06j with $f_{\rm o1}$ at 3.4 GHz. Since the transmission line considered here is dissipation-free, if there is a transition from capacitive reactance to inductive reactance, then there must exist a point where $Y_{\rm in}^{\rm o}$ is equal to 0, and therefore W_5 takes 3.2 mm. The even-mode circuit can be analyzed similarly. The input impedance of the even-mode circuit is expressed via Eqs. (10)–(15), and $Z_{\rm in}^{\rm e}=0$ is given as the even-mode resonance condition. Using interpolation again, with $f_{\rm e1}$ at 5 GHz, it is observed that when W_5 changes near 3.9 mm, $Z_{\rm in}^{\rm e}$ shifts from -1.5j to 2.18j, so W_5 chooses 3.9 mm. Finally, W_5 takes a mean value 3.55 mm of 3.2 mm and 3.9 mm, indicating the completion of the first-round interpolation (θ_2 determined).

$$
\begin{aligned}
{}^{\rm III}Y_{11}^{\rm e} &= {\rm j}2Y_2\frac{3\sin((5/2)\theta_2+\theta_4+\theta_5)+\sin((3/2)\theta_2+\theta_4-\theta_5)+\sin((3/2)\theta_2-\theta_4+\theta_5)-\sin((1/2)\theta_2-\theta_4-\theta_5)}{3\cos((5/2)\theta_2+\theta_4+\theta_5)+\cos((3/2)\theta_2+\theta_4-\theta_5)+\cos((3/2)\theta_2-\theta_4+\theta_5)-\cos((1/2)\theta_2-\theta_4-\theta_5)}\\
&\quad+{\rm j}2Y_2\tan\theta_3, \qquad (10)\\
{}^{\rm III}Y_{12}^{\rm e} &= {}^{\rm III}Y_{21}^{\rm e}=\frac{-{\rm j}4Y_2[2\sin((1/2)\theta_2+\theta_4+\theta_5)-\sin((1/2)\theta_2-\theta_4+\theta_5)-\sin((1/2)\theta_2+\theta_4-\theta_5)]}{3\cos((5/2)\theta_2+\theta_4+\theta_5)+\cos((3/2)\theta_2+\theta_4-\theta_5)+\cos((3/2)\theta_2-\theta_4+\theta_5)-\cos((1/2)\theta_2-\theta_4-\theta_5)}\\
&\quad-{\rm j}2Y_2\tan\theta_3, \qquad (11)\\
{}^{\rm III}Y_{22}^{\rm e} &= \frac{{\rm j}2Y_2(3\cos 2\theta_2-\cos\theta_2)[2\sin((1/2)\theta_2+\theta_4+\theta_5)-\sin((1/2)\theta_2-\theta_4+\theta_5)-\sin((1/2)\theta_2+\theta_4-\theta_5)]}{3\cos((5/2)\theta_2+\theta_4+\theta_5)+\cos((3/2)\theta_2+\theta_4-\theta_5)+\cos((3/2)\theta_2-\theta_4+\theta_5)-\cos((1/2)\theta_2-\theta_4-\theta_5)}\\
&\quad+{\rm j}2Y_2\tan\theta_3, \qquad (12)
\end{aligned}
$$

$$
M_{\rm III}^{\rm e}=\frac{1}{{}^{\rm III}Y_{21}^{\rm e}}\begin{bmatrix}-{}^{\rm III}Y_{22}^{\rm e} & -1\\ {}^{\rm III}Y_{12}^{\rm e}\,{}^{\rm III}Y_{21}^{\rm e}-{}^{\rm III}Y_{11}^{\rm e}\,{}^{\rm III}Y_{22}^{\rm e} & -{}^{\rm III}Y_{11}^{\rm e}\end{bmatrix}, \qquad (13)
$$

$$
M_{[ABCD]}^{\rm e}=M_{\rm I}\cdot M_{\rm II}\cdot M_{\rm III}^{\rm e}, \qquad (14)
$$

$$
Z_{\rm in}^{\rm e}=\frac{M_{[A]}^{\rm e}}{M_{[C]}^{\rm e}}, \qquad (15)
$$

$$
Y_{\rm in}^{\rm e}=\frac{M_{[D]}^{\rm e}}{M_{[B]}^{\rm e}}, \qquad (16)
$$

$$
S_{21}=Y_0\left(Y_{\rm in}^{\rm o}-Y_{\rm in}^{\rm e}\right)/\left[\left(Y_0+Y_{\rm in}^{\rm o}\right)\left(Y_0+Y_{\rm in}^{\rm e}\right)\right], \qquad (17)
$$

$$
Y_{\rm in}=Y_0\frac{Y_L+{\rm j}Y_0\tan\theta}{Y_0+{\rm j}Y_L\tan\theta}. \qquad (18)
$$

The second-round interpolation is based on the first round. Here, B_4 is adjusted to 1.4 for optimizing the reflection around the central frequency, because it is found that the reflection at the high frequency is better than that at the low frequency when ICL is simulated separately, which indicates that the center frequency corresponding to ICL is relatively high. There are usually high-order modes located in the upper stopband in the UWB filter designs, and it is necessary to introduce TZs to suppress them. For example, $f_{\rm o4}$ (15.4 GHz) here is situated in the upper stopband. From Eq. (17) we know that a TZ can be generated when $Y_{\rm in}^{\rm o}=Y_{\rm in}^{\rm e}$, and $Y_{\rm in}^{\rm o}$ and $Y_{\rm in}^{\rm e}$ are given by Eqs. (8) and (16). Therefore, by interpolating near B_1, B_2, and B_3 (0.4, 0.3, and 1), TZs are introduced to reject $f_{\rm o4}$ and improve the selectivity. The final values for B_1, B_2, and B_3 are shown in Table 3.

The TZs generated by the stepped-impedance stubs are related to the frequencies of the resonances. The loaded stepped-impedance stubs can not only generate the resonances through the first round of interpolation but also can adjust the TZ frequency through the second round of interpolation. In other words, the stepped-impedance stubs affect both the resonance frequency and the TZ frequency. When the electrical lengths of the centrally-loaded stubs are a quarter of the wavelength, the center of the resonator can be equivalent to grounding, and therefore a TZ can be generated. And the frequency of the TZ can be derived from

$$
Y_{\rm a}=-{\rm j}Y_{i1}\cot\theta_{i1}, \qquad (19)
$$

$$
Y_{\rm b}=Y_{i2}\frac{-{\rm j}Y_{i1}\cot\theta_{i1}+{\rm j}Y_{i2}\tan\theta_{i2}}{Y_{i2}+Y_{i1}\cot\theta_{i1}\tan\theta_{i2}}=0\quad(i=1,2,3). \qquad (20)
$$

Table 3. Initial values for proposed UWB filter.

Y_0/θ_0	Y_1/θ_1	Y_2/θ_2	Y_{31}/θ_{31}	Y_{32}/θ_{32}	Y_{41}/θ_{41}
0.02/1.35	0.01/2.13	0.014/1.59	0.014/0.3	0.022/0.22	0.01/0.21
Y_{42}/θ_{42}	Y_{51}/θ_{51}	Y_{52}/θ_{52}	$K_1/K_2/K_3$	$B_1/B_2/B_3/B_4$	
0.02/0.22	0.014/0.14	0.035/0.49	1/0.5/1	0.39/0.28/0.62/1.4	

Here, the TZs generated by the stepped-impedance stubs are computed to be 13.5 GHz, 17.13 GHz, and 20 GHz, respectively. Note that the parasitic effect of the microstrip line and the mutual coupling of the filter structure itself cannot be ignored due to the high stopband frequency.

Finally, the uniform-impedance stubs are converted into the stepped-impedance ones, where a high-impedance ratio is

employed for miniaturization. The low-impedance line parameters are given according to Eq. (17), with the high-impedance line parameters fixed. All the initial values of the proposed UWB filter are listed in Table 3, where the electrical lengths are all based on the center frequency. It should be noted that B_1, B_2, and B_3 have infinite solutions, and only one set of solutions is given here. The two-round interpolation method used here can be applied to other odd–even-mode filter designs where the conditions of odd- and even-mode resonances and TZs generation are required to be analyzed. This approach can effectively improve the design efficiency by reducing complex calculations while ensuring relatively high accuracy.

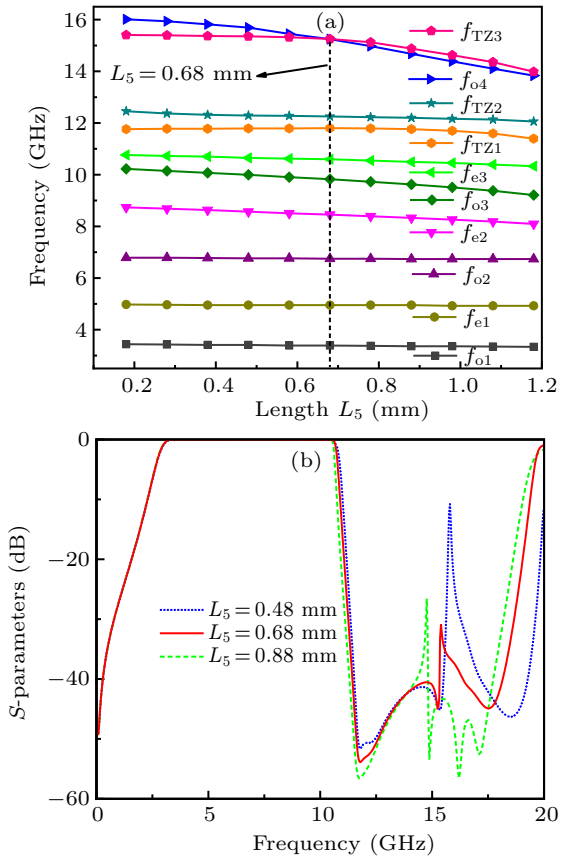


Fig. 4. (a) Changing trends of even and odd modes and TZs with L_5, and (b) S-parameter varying with frequency for three values of L_5 on the high-order mode f_{o4}.

The proposed filter has the characteristic of a wide upper rejection band, and the parameter L_5 is especially important in suppressing the out-of-band spurious perturbation. The value of L_5 can be obtained by converting the uniform-impedance stub into the stepped-impedance one. The input admittance of the uniform-impedance stub is Y_3 and that of the stepped-impedance one is Y_b. $Y_3 = 0.014$ S, and the electrical length $\theta_3 = 0.64$. To facilitate the design and processing, the physical dimensions of the stepped-impedance stub are set to be $W_6 = 0.2$ mm, $W_7 = 0.6$ mm, and $L_6 = 0.5$ mm. By converting these dimensions into the electrical lengths, which are subsequently substituted into Eqs. (20)–(23), we obtain $\theta_{31} = 0.31$, and then we convert θ_{31} (L_5) into a physical size of 0.7 mm again.

$$Y = \mathrm{j}Y_3 \tan\theta_3, \tag{21}$$

$$Y_a = \mathrm{j}Y_{31} \tan\theta_{31}, \tag{22}$$

$$Y_b = Y_{32}\frac{\mathrm{j}Y_{31}\tan\theta_{31} + \mathrm{j}Y_{32}\tan\theta_{32}}{Y_{32} - Y_{31}\tan\theta_{31}\tan\theta_{32}}, \tag{23}$$

$$Y = Y_b. \tag{24}$$

Through the above analysis and calculations, all the initial values are obtained. To further verify the reliability of the two-round interpolation approach, verification through simulation is conducted. The important parameter L_5 is selected here to perform the verification. Let L_5 take multiple values, so that the changing trends of resonance modes and TZs are more intuitive as shown in Fig. 4(a). When L_5 is equal to around 0.68 mm, f_{04} and f_{TZ3} coincide, which means that f_{04} is rejected by f_{TZ3}. This high-mode suppression effect can also be observed in Fig. 4(b). And according to the above calculation, L_5 is 0.7 mm, indicating the good agreement between simulation and theoretical calculation, which confirms the reliability of the two-round interpolation method.

3. Fabrication and measurements

The proposed UWB filter is designed and optimized by full-wave electromagnetic simulation software IE3D, and the finally obtained optimal dimensions are listed in the caption of Fig. 6. According to the filter pattern on the mask, the corresponding circuit is etched on the 0.5-mm-thick YBCO/MgO/YBCO high-temperature superconducting thin film with a size of 25.10 mm × 13.63 mm and a dielectric constant of 9.8 by the photolithography technology. Figure 5 shows the fabricated filter consisting of a superconducting thin-film circuit, metal shielding box, and SMA connectors. To ensure a good electrical connection between the circuit and the pins of the connectors, the gold covered on the 50-Ω microstrip line is reserved.

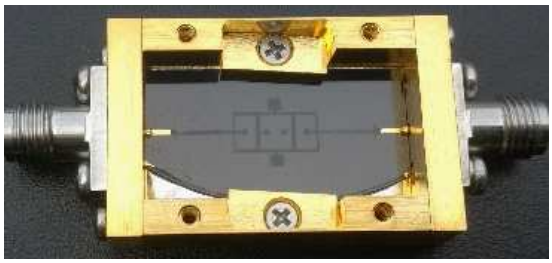


Fig. 5. Fabricated HTS UWB filter.

Figure 6 shows the test and simulation responses of the filter. The transmission poles in the passband are changed from six to eight due to the utilization of ICL.[6] The measured results are well consistent with the simulated ones. The passband covers 3.1 GHz–10.6 GHz; the maximum insertion loss within the passband is only 0.42 dB, and the reflection is better than −15.6 dB. The upper stopband with attenuation greater than 25 dB extends to 19 GHz, and most of the upper

stopband is inhibited to approximately −40 dB. Besides, the in-band group delay is less than 2 ns.

Table 4 presents the comparison of the filter proposed in this work with the single-stage multi-mode UWB filters in other references. Our filter shows superiority in the insertion loss, return loss, and upper stopband rejection characteristics.

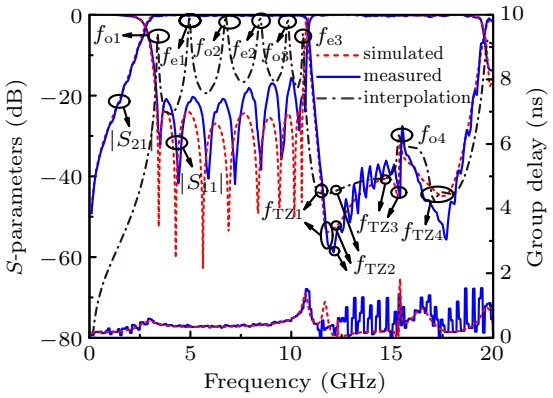


Fig. 6. Simulated and measured results. The finally obtained dimensions are as follows: $W_1 = 0.48$, $W_2 = 0.11$, $W_3 = 0.07$, $W_4 = 0.12$, $W_5 = 3.96$, $W_6 = 0.17$, $W_7 = 0.58$, $W_8 = 0.10$, $W_9 = 0.48$, $W_{10} = 0.20$, $W_{11} = 1.27$, $L_1 = 3.00$, $L_2 = 5.12$, $L_3 = 4.74$, $L_4 = 8.13$, $L_5 = 0.68$, $L_6 = 0.50$, $L_7 = 2.02$, $L_8 = 3.06$, $L_9 = 0.47$, $L_{10} = 0.50$, $h_1 = 0.47$, $h_2 = 0.55$, $h_3 = 0.31$, $h_4 = 1.09$, and $S_1 = 0.03$ (all in units of mm).

Table 4. Comparison of our proposed filter with the reported UWB filters.

Ref.	IL (dB)	RL (dB)	Material	3-dB FBW (%)	Number of resonances	Rejection level (dB)
[13]	< 0.9	13.0	copper	110.9	4	around 25
[14]	< 1.30	10.6	HTS	111.0	7	around 26
[15]	< 1.60	12.0	copper	110.1	7	around 28
Our	< 0.42	15.6	HTS	109.5	8	around 40

IL: maximum in-band insertion loss; RL: return loss; 3-dB FBW: 3-dB fractional bandwidth of passband; rejection level: upper stopband rejection level.

4. Conclusions

Based on the ring resonator and stepped-impedance open stubs, a sextuple-mode ring resonator is proposed and used in a single-stage UWB filter design. The good in-band return loss, right band-edge selectivity, and upper stopband rejection are achieved because of the efficacy of this resonator and ICL structure. The proposed two-round interpolation method exhibits the practicability in the odd–even-mode filter designs.

References

[1] Kheir M, Kroger T and Hoft M 2017 *IEEE Access* **5** 1714
[2] Tan B T, Yu J J, Chew S T, Leong M S and Ooi B L 2005 *IEEE Trans. Microw. Theory Tech.* **53** 343
[3] Chiou Y C, Kuo J T and Wu J S 2008 *IEEE Microw. Wirel. Compon. Lett.* **18** 97
[4] Lok U H, Chiou Y C and Kuo J T 2008 *IEEE Microw. Wirel. Compon. Lett.* **18** 179
[5] Kundu A C and Awai I 2001 *IEEE Trans. Microw. Theory Tech.* **49** 1113
[6] Kim C H and Chang K 2011 *IEEE Microw. Wirel. Compon. Lett.* **21** 206
[7] Sun S and Zhu L 2007 *IEEE Trans. Microw. Theory Tech.* **55** 2176
[8] Liu H, Ren B, Guan X, Lei J and Li S 2013 *IEEE Microw. Wirel. Compon. Lett.* **23** 181
[9] Shi J, Lin L, Chen J X, Chu H and Wu X 2014 *IEEE Microw. Wirel. Compon. Lett.* **24** 442
[10] Kumar S, Gupta R D and Parihar M S 2016 *IEEE Microw. Wirel. Compon. Lett.* **26** 340
[11] Taibi A, Trabelsi M, Slimane A, Belaroussi M T and Raskin J P 2015 *IEEE Microw. Wirel. Compon. Lett.* **25** 4
[12] Sahin E G , Gorur A K , Karpuz C , and Gorur A 2019 *49th European Microwave Conference (EuMC)*, October 1–3, 2019, Paris, France, p. 464
[13] Zeng J, Li X and Qi Z 2019 *Microw. Opt. Technol. Lett.* **62** 1521
[14] Shang Z, Guo X, Cao B, Wei B and Song X 2013 *IEEE Microw. Wirel. Compon. Lett.* **23** 72
[15] Zhou C X, Guo P P, Zhou K and Wu W 2017 *IEEE Microw. Wirel. Compon. Lett.* **27** 636